Theoretical Study of Local Electronic Alloy Effects of OOH, OH, and O Adsorption on Pt–Pd Cluster Model

ARTICLE *in* THE JOURNAL OF PHYSICAL CHEMISTRY C · APRIL 2011

Impact Factor: 4.77 · DOI: 10.1021/jp2000859

4 AUTHORS, INCLUDING:

Shyi-Long Lee
National Chung Cheng University
199 PUBLICATIONS **1,691** CITATIONS

THE JOURNAL OF PHYSICAL CHEMISTRY C

ARTICLE

pubs.acs.org/JPCC

Theoretical Study of Local Electronic Alloy Effects of OOH, OH, and O Adsorption on Pt−Pd Cluster Model

Yu-Wei Huang, Ting-Yi Chou, Guan-Yi Yu, and Shyi-Long Lee*

Department of Chemistry and Biochemistry, National Chung-Cheng University, Chia-Yi 621, Taiwan

Supporting Information

ABSTRACT: The local electronic alloy effects of OOH, OH, and O adsorption on Pt−Pd alloy clusters have been investigated by the density functional theory method. Such investigation on the local electronic alloy effect will enhance the supported Pt-based catalyst to study the catalytic ability of oxygen reduction reaction (ORR). In our current investigation, the 8 cluster models containing 15 atoms were constructed to check the alloy influence of central, surrounding, and subsurface replacing effect. It has been observed that the adsorption energies of OOH and OH are reduced upon replacing the two central Pt atoms by Pd atoms or the subsurface Pt layer by Pd layer and enhanced upon replacing the surrounding Pt atom circle by Pd atom circle. The adsorption energy of O is enhanced upon replacing the two central Pt atoms by Pd atoms or the surrounding Pt atom circle by Pd atom circle and reduced after replacing the subsurface Pt layer by Pd layer. The different adsorption behavior can be rationalized by examining their bonding picture through analysis of the atom-projected density of states and overlap population density of states. The Pt-surrounded Pd configuration D may be the best choice for ORR since it weakens the OH adsorption the most and thus reduces the poisoning of ORR active site.

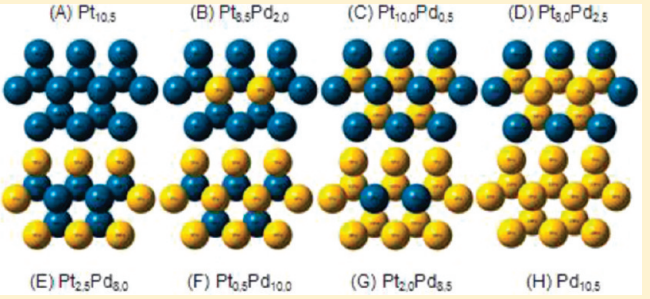

1. INTRODUCTION

Catalytic reactions of fuel cells long have been a subject of great research interest because of their fundamental and industrial importance.[1] To improve the fuel cell efficiency, there are several challenging issues worth being studied. These include the slow cathode kinetics of oxygen reduction reaction (ORR)[1−4] and the high price for Pt metal which is the best catalyst for H_2 and O_2 dissociation. Recently, the supported Pt-based alloy catalyst has received great attention because of its wide variety of advantages. In this paper, we would like to report our recent studies of O, OH, and OOH adsorption on Pt/Pd using cluster model calculation.

Recent experimental observations showed that the Pt-based alloys on supported materials can largely enhance the catalytic ability of ORR.[5−13] For example, the ORR activity on carbon-supported Pt−Pd alloy is 5−8 times higher than that on carbon-supported pure Pt catalyst.[12] This can be explained by a well-known fact: the configuration of alloy can strongly modify the properties of materials.[14] Besides, some experimental[3,13,15] and theoretical[16−20] results also reported that the Pt-skin configuration can effectively improve the ORR activity. This indicates that different alloy configurations could have some extra effects on adsorption processes. It would be interesting to further explore such a local electronic effect on Pt−Pd alloy nanoclusters of different configurations for ORR.

Although most calculations[16−20] on crystalline surface processes were done on the slab model, for our purpose, it is hard to apply this approach to discuss the pure local electronic effect of alloy cluster due to lack of the periodicity. Moreover, it allows a more direct analysis of the bonding character for local orbitals. Hence, the cluster model is a suitable model to be used in this study.

It has been reported that the ORR favors to process the direct four-electron reduction mechanism for Pt and Pt-based catalyst. The O, OH, and OOH adsorbates are three important intermediates for the four-electron reduction mechanism. It has long been recognized that the origin of slow ORR kinetics is the blockage of O_2 adsorption sites by the formation of O and OH.[21,22] Hence the studies of O, OH, and OOH adsorption are important for ORR research. The main objective of this study is to provide a systematic way to describe how the electronic configurations of Pt−Pd alloy catalyst affect the adsorption behaviors of three adsorbates.

In section 2, a brief description of the computational method and cluster construction are given. In section 3, the results and discussion of the adsorption energies and electronic structures on different alloy configurations are presented. Conclusions are drawn in the final section.

2. COMPUTATIONAL DETAILS

In order to mimic different Pt−Pd alloy surfaces, 8 cluster models containing 15 atoms $Pt_{10,5}$ (A), $Pt_{8,5}Pd_{2,0}$ (B), $Pt_{10,0}Pd_{0,5}$

Received: January 4, 2011
Revised: March 24, 2011
Published: April 20, 2011

dx.doi.org/10.1021/jp2000859 | J. Phys. Chem. C 2011, 115, 9105–9116

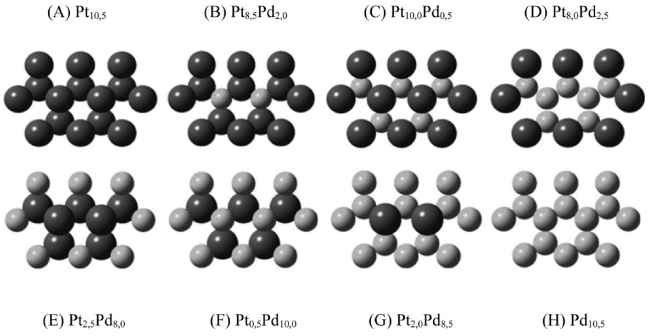

Figure 1. Eight different configurations for Pt−Pd alloy cluster.

(C), $Pt_{8,0}Pd_{2,5}$ (D), $Pt_{2,5}Pd_{8,0}$ (E), $Pt_{0,5}Pd_{10,0}$ (F), $Pt_{2,0}Pd_{8,5}$ (G), and $Pd_{10,5}$ (H) were constructed and are shown in Figure 1. By using these eight alloy clusters, one can discuss the effect of replacing two Pt atoms by two Pd atoms at the active center of the first layer by comparing (A−B), (C−D), (E−F), and (G−H). We called this the center-replacing effect. A second effect called surrounding-replacing effect can also be discussed by comparing (A−E), (B−F), (C−G), and (D−H). Finally, we can also examine the effect called subsurface-replacing effect by comparing (A−C), (B−D), (E−G), and (F−H).

The hybrid B3LYP functional was applied in the calculation.[23] The LANL2DZ basis sets as well as effective core potentials were used for platinum and palladium atoms, and the 6-31G* basis sets were used for oxygen and hydrogen atoms.[24,25] The electronic configurations for Pd and Pt metals are $[Kr]4d^{10}$ and $[Xe]-4f^{14}5d^{9}6s^{1}$. Because the LANL2DZ basis sets with effective core potential are used in this study, only 4s4p4d5s and 5s5p5d6s orbitals are considered for Pd and Pt, respectively.

The geometry of alloy cluster was fixed during the geometry optimization, and the metal−metal length d is determined by[26]

$$d = \frac{n_{Pt} \times 2.775 + n_{Pd} \times 2.751}{n_{Pt} + n_{Pd}} \quad (1)$$

where n_{Pt} and n_{Pd} are the number of Pt and Pd atoms, respectively, and d is the metal−metal distance. Adsorbate O, OH, and OOH can then be adsorbed on Pt_nPd_m. All possible spin multiplicities were considered to determine the electronic configuration of the ground adsorbed state. The adsorption energy E_{ad} is obtained according to

$$E_{ads} = E_{tot} - E_{surface} - E_{adsorbate} \quad (2)$$

where E_{tot} is the total energy of adsorbed Pt−Pd alloy cluster, E_{surf} is the total energy of bare alloy cluster, and $E_{adsorbate}$ is the total energy of adsorbate. The geometry optimization and orbital analysis were performed with the program package GAUSSIAN 03.[27] The surface atom-projected density of states and overlap population density of states were computed based on the orbital analysis of Mulliken formulation by using the AOMIX software 6.46.[28,29]

3. RESULTS AND DISCUSSION

3.1. Bare Alloy Clusters. The total energies, multiplicities, cohesive energies of bare Pt−Pd alloy clusters (see Figure 1) are summarized in Table 1. For pure metal cluster $Pt_{10,5}$ and $Pd_{10,5}$, the most stable spin states are $M = 13$ and $M = 7$, respectively. For other alloy clusters, the most stable spin states are between $M = 7$ and $M = 13$. The details of energies for other spin states are provided in the Supporting Information. The cohesive energy E_c is defined as

Table 1. Total Energies, Multiplicity, Cohesive Energies, and Charges of Pt−Pd Alloy Clusters

	total energy	multiplicity	cohesive energy	$q(M)^a$
$Pt_{10,5}$ (A)	−1787.62110	13	−2.64	0.30
$Pt_{8,5}Pd_{2,0}$ (B)	−1802.79665	11	−2.49	0.73
$Pt_{10,0}Pd_{0,5}$ (C)	−1825.59915	11	−2.34	0.58
$Pt_{8,0}Pd_{2,5}$ (D)	−1840.77180	9	−2.18	0.97
$Pt_{2,5}Pd_{8,0}$ (E)	−1848.36623	9	−2.12	−0.18
$Pt_{0,5}Pd_{10,0}$ (F)	−1863.53243	9	−1.95	−0.01
$Pt_{2,0}Pd_{8,5}$ (G)	−1886.32851	7	−1.79	0.00
$Pd_{10,5}$ (H)	−1901.49011	7	−1.61	0.11

[a] The average Mulliken charge for two center metal atoms.

$$E_c = \frac{E_{tot} - n_{Pt}E_{Pt} - n_{Pd}E_{Pd}}{15} \quad (3)$$

where E_{Pt} and E_{Pd} are the total energies of the isolated metal atom with the most stable spin state, and E_{tot} is the total energy of alloy cluster. It can be found that the cohesive energy of alloy cluster is proportional to the ratio of Pt component. The average Mulliken charges for two central atoms are also shown in Table 1. For the pure Pt and Pd clusters, the average Mulliken charges are 0.30 and 0.11, respectively. The largest and smallest charges occur for the two mixed configurations, $Pt_{8,0}Pd_{2,5}$ (D) and $Pt_{2,5}Pd_{8,0}$ (E), respectively. Upon replacing the active-site Pt atoms by Pd atoms, the Pd atoms are more positive than Pt atoms. Upon replacing the surrounding Pt atom circle by Pd atom circle, the active-site metal atoms are more negative. Upon replacing the subsurface Pt layer by Pd layer, the active-site metal atoms are more positive.

3.2. The O, OH, and OOH Adsorption on Pt−Pd Alloy Clusters. Table 2 collects the ground state spin multiplicity, square of the total spin angular momenta, adsorption energies, bond lengths, and Mulliken charges of OOH adsorption on various Pt−Pd alloy clusters. As can be seen in Table 2, OOH adsorptions on the Pd-skin configuration, i.e., $Pt_{0,5}Pd_{10,0}$ (F), and Pd-surrounded Pt configuration, i.e., $Pt_{2,5}Pd_{8,0}$ (E), are stronger than those on other configurations. The weakest adsorption for OOH occurs in the Pt-surrounded Pd configuration $Pt_{8,0}Pd_{2,5}$ (D). For the Pt-skin $Pt_{10,0}Pd_{0,5}$ (C) configuration, the adsorption energy for OOH is weaker than that for pure Pt (A) or Pd (H) clusters. Our results agree very well with those of recent DFT slab model calculation[19] showing that OOH would not favor to adsorb on the Pt-skin configuration.

For the isolated OOH molecule, the OO−H bond length is 0.98 Å. It is found that the OO−H length is not changed upon adsorption on all Pt−Pd alloy clusters. However, the O−O bond length is found to be lengthened observably by 0.07−0.15 Å compared to the isolated O−O bond length of 1.33 Å. As can be seen in Table 2, the larger O−O bond lengthening in the case of E and F and the smallest in the case of D agree well with the trend in adsorption energy. It can be found that the O−O bond lengths for OOH adsorption increase with the enhancement of OOH adsorption and thus favor OOH dissociation.

For the bond lengths M−O and M−OH of OOH adsorption, the bond lengths M−OH are longer than M−O reflecting a weaker bonding in M−OH. M−O bond length varies slightly,

dx.doi.org/10.1021/jp2000859 |J. Phys. Chem. C 2011, 115, 9105–9116

Table 2. Spin Multiplicity, Square of the Total Spin Angular Momenta, Adsorption Energies, Bond Lengths, and Mullikan Charges of the OOH Adsorption on Pt−Pd Alloy Clusters

	M	$/S^2/^a$	E_{ads}(eV)	r(M_2-O)	r(M_3−OH)	r(O−O)	r(O−H)	q(O_{16})	q(O_{17})	q(H_{18})
$Pt_{10,5}$ (A)	12	35.94(35.75)	−0.82	2.02	2.49	1.45	0.98	−0.30	−0.33	0.49
$Pt_{8,5}Pd_{2,0}$ (B)	12	35.97(35.75)	−0.71	2.01	2.49	1.43	0.98	−0.26	−0.32	0.48
$Pt_{10,0}Pd_{0,5}$ (C)	12	35.90(35.75)	−0.71	2.08	2.49	1.45	0.98	−0.28	−0.33	0.49
$Pt_{8,0}Pd_{2,5}$ (D)	10	25.09(24.77)	−0.40	2.00	2.69	1.40	0.98	−0.23	−0.30	0.48
$Pt_{2,5}Pd_{8,0}$ (E)	4	4.98(4.62)	−1.16	2.03	2.23	1.48	0.98	−0.31	−0.36	0.50
$Pt_{0,5}Pd_{10,0}$ (F)	8	15.98(15.75)	−1.17	2.05	2.27	1.47	0.98	−0.29	−0.36	0.48
$Pt_{2,0}Pd_{8,5}$ (G)	6	8.98(8.77)	−0.93	2.02	2.55	1.45	0.98	−0.31	−0.33	0.49
$Pd_{10,5}$ (H)	6	5.42(5.07)	−0.86	2.03	2.35	1.44	0.98	−0.27	−0.34	0.48

[a] The square of the total spin angular momenta before(after) spin annihilation.

Table 3. Spin Multiplicity, Square of the Total Spin Angular Momenta, Adsorption Energies, Bond Lengths, and Mullikan Charges of the OH Adsorption on Pt−Pd Alloy Clusters

	M	$/S^2/^a$	E_{ads}(eV)	r(M_3−O)	r(O−H)	∠(M_3−O−H)	q(O_{16})	q(H_{17})
$Pt_{10,5}$ (A)	12	35.92(35.75)	−1.84	2.01	0.97	105.3	−0.63	0.46
$Pt_{8,5}Pd_{2,0}$ (B)	12	35.95(35.75)	−1.61	2.01	0.97	105.4	−0.60	0.44
$Pt_{10,0}Pd_{0,5}$ (C)	12	24.48(24.79)	−1.70	2.04	0.97	105.9	−0.63	0.45
$Pt_{8,0}Pd_{2,5}$ (D)	6	11.15(11.13)	−1.10	1.98	0.97	103.7	−0.59	0.45
$Pt_{2,5}Pd_{8,0}$ (E)	6	9.65(8.87)	−2.22	1.99	0.98	106.6	−0.66	0.46
$Pt_{0,5}Pd_{10,0}$ (F)	8	15.94(15.76)	−2.03	1.99	0.97	105.4	−0.63	0.43
$Pt_{2,0}Pd_{8,5}$ (G)	8	15.94(1576)	−2.00	2.02	0.97	106.8	−0.66	0.46
$Pd_{10,5}$ (H)	8	15.94(15.76)	−1.75	2.03	0.97	106.7	−0.63	0.43

[a] The square of the total spin angular momenta before(after) spin annihilation.

i.e., within 0.08 Å among 8 configurations, while a larger deviation of 0.46 Å is found in M−OH bond length. As can be seen in Table 2, M−O bond length is averaged shorter slightly upon adsorption on Pt atom than on Pd atom. It is interesting to notice that shorter M−OH bond lengths for Pd-surrounded $Pt_{2,5}Pd_{8,0}$ (E) and Pd-skin $Pt_{0,5}Pd_{10,0}$ (F) configuration result in the stronger adsorption of OOH while the longest M−OH bond length for Pt-surrounded Pd configuration $Pt_{8,0}Pd_{2,5}$ (D) results in the weakest adsorption of OOH.

Table 3 collects the ground state spin multiplicity, square of the total spin angular momenta, adsorption energies, bond lengths, and Mulliken charges of OH adsorption on various Pt−Pd alloy clusters. It is found that the OH adsorption on the Pd-surrounded Pt configuration $Pt_{2,5}Pd_{8,0}$ (E) is stronger than those on other configurations. The weakest adsorption for OH occurs in the Pt-surrounded Pd configuration $Pt_{8,0}Pd_{2,5}$ (D). This trend is similar to those obtained for OOH adsorption. For the Pt-skin $Pt_{10,0}Pd_{0,5}$ (C) configuration, the adsorption energy for OH is weaker than that for pure Pt (A) or Pd (H) clusters. Our results also agree very well with those of recent DFT slab model calculation[19] showing that OH would not favor to adsorb on the Pt-skin configuration.

For the isolated OH molecule, the O−H bond length is 0.98 Å. As can be seen in Table 3, the O−H length is only slightly reduced around 0.01 Å. For the bond length M−O of OH adsorption, the two smallest M−O bond lengths are for Pt-surrounded Pd configuration $Pt_{8,0}Pd_{2,5}$ (D) with weakest adsorption energy and Pd-surrounded Pt configuration $Pt_{2,5}Pd_{8,0}$ (E) with strongest adsorption energy. Thus, the lengths of M−O are not able to reflect on the OH adsorption strength. However, the angle M_3−O−H for D configuration is smaller compared to other configurations; it shows that the D configuration possesses peculiar local electronic properties with respect to other configurations and corresponds to the smallest adsorption energy.

Table 4. Spin Multiplicity, Square of the Total Spin Angular Momenta, Adsorption Energies, Bond Lengths, and Mullikan Charges of the O Adsorption on Pt−Pd Alloy Clusters

	M	$/S^2/^b$	E_{ads}(eV)	r(S−O)[a]	q(O)
$Pt_{10,5}$ (A)	13	42.17(42.00)	−2.49	1.32	−0.52
$Pt_{8,5}Pd_{2,0}$ (B)	11	30.29(30.01)	−2.67	1.20	−0.55
$Pt_{10,0}Pd_{0,5}$ (C)	11	30.17(30.00)	−2.54	1.32	−0.50
$Pt_{8,0}Pd_{2,5}$ (D)	7	13.26(12.30)	−2.62	1.19	−0.56
$Pt_{2,5}Pd_{8,0}$ (E)	9	20.23(20.01)	−3.18	1.28	−0.53
$Pt_{0,5}Pd_{10,0}$ (F)	9	20.23(20.01)	−3.19	1.26	−0.53
$Pt_{2,0}Pd_{8,5}$ (G)	5	7.18(6.33)	−2.95	1.26	−0.50
$Pd_{10,5}$ (H)	7	12.30(12.02)	−3.21	1.23	−0.52

[a] The length between the metal surface and oxygen. [b] The square of the total spin angular momenta before(after) spin annihilation.

Table 4 collects the ground state spin multiplicity, square of the total spin angular momenta, adsorption energies, bond lengths, and Mulliken charges of O adsorption on various Pt−Pd alloy clusters. It is found the O adsorption on the pure Pd (H) cluster is stronger than those on other configurations. The weakest adsorption for O occurs in the pure Pt (A) cluster.

For the O adsorption, the shortest oxygen−surface (O−S) length is 1.19 Å for Pt-surrounded Pd configuration $Pt_{8,0}Pd_{2,5}$ (D) configuration, and the longest O−S bond length 1.32 Å is for pure Pt (A) and Pd-skin $Pt_{0,5}Pd_{10,0}$ (G) configuration. No observable relationship between the adsorption energy and O−S length can be seen.

dx.doi.org/10.1021/jp2000859 |J. Phys. Chem. C 2011, 115, 9105–9116

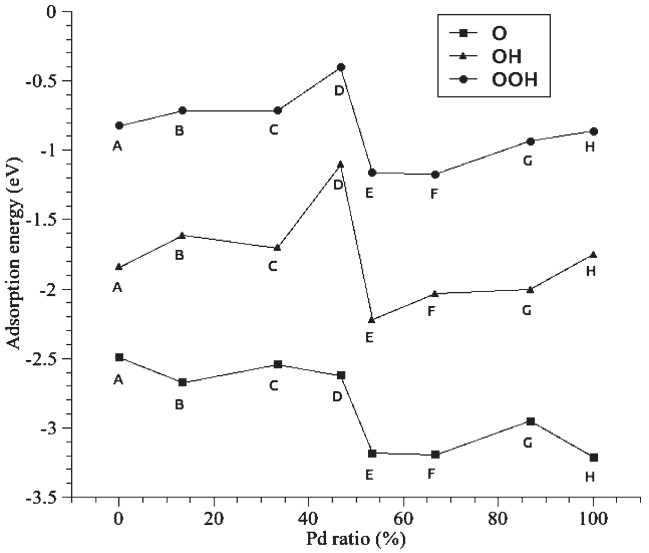

Figure 2. Adsorption energies of O, OH, and OOH as a function of Pd composition ratio.

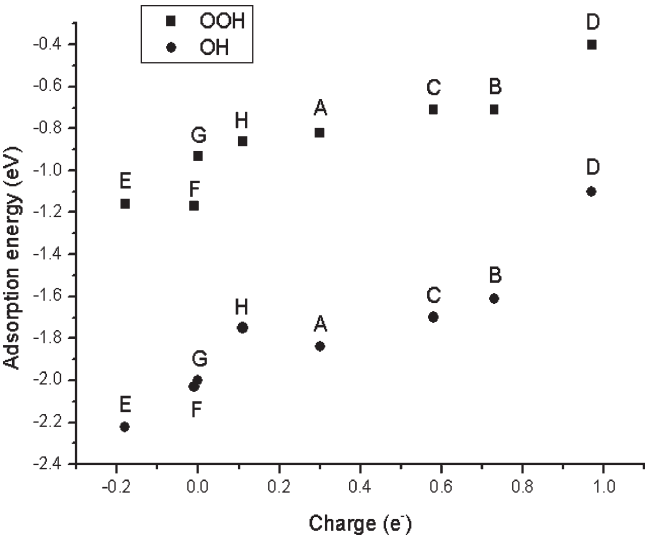

Figure 3. Adsorption energies of OH and OOH as a function of average charges for two center atoms.

As mentioned earlier, it is well-known that many physical properties of alloys, like Fermi level and optical properties, are dependent on the alloy composition ratio. However, it might not be true for chemical reactions occurring on alloy surfaces. Figure 2 shows the adsorption energies of O, OH, and OOH as a function of alloy composition ratio. As can be seen in Figure 2, the adsorption energy is not dependent on the alloy composition ratio.

Figure 3 shows the adsorption energies of OH and OOH as a function of average charges for the two central metal atoms. As can be seen in Figure 3, the linear relationship between the average charges and adsorption energies indicates that the charge content at the two central metal atoms would affect the OH and OOH adsorption. This extra effect is essentially derived from local structure, and detailed analysis is needed, which has been described in the following section.

In order to further discuss the alloy effect of local structure on adsorption, we consider the differences of adsorption energy, charge, bond lengths, and Fermi level, as well as d-band centers for various alloy configurations in Tables 2, 3, and 4. As can be seen from Table 2− 4, the OOH adsorptions are stronger when replacing the two central Pt atoms by Pd atoms, replacing the eight surrounding Pt atoms by Pd atoms, and replacing five subsurface Pd atoms by Pt atoms. The O−O bond length is reduced when replacing the two central Pt atoms by Pd atoms and replacing the subsurface Pt layer by Pd layer but is lengthened when replacing the surrounding Pt atom circle by Pd atom circle. For the M−OH and M−O lengths, no observable regularity of replacement effect can be seen. For the Mulliken charge $q(O_1)$, it is increased when replacing the two center Pt atoms by Pd atoms and replacing the subsurface Pt layer by Pd layer and then decreased when replacing the surrounding Pt atom circle by Pd atom circle. For the Mulliken charge $q(O_2)$, it is increased when replacing the subsurface Pt layer by Pd layer and then decreased when replacing the surrounding Pt atom circle by Pd atom circle. No observable regularity of center-replacing effect can be seen. For the Mulliken charge $q(H)$, although the effect is small, it still can be found that the charge is decreased when replacing the two center Pt atoms by Pd atoms and replacing the subsurface Pt layer by Pd layer, and increased when replacing the surrounding Pt atom circle by Pd atom circle.

In the case of OH adsorption, it is stronger when replacing the two central Pd atoms by Pt atoms, replacing the eight surrounding Pt atoms by Pd atoms, and replacing five subsurface Pd atoms by Pt atoms. It can also be seen that the M−O−H angle is reduced when replacing two central Pt atoms by Pd atoms, and the bond angle is raised when replacing surrounding Pt atom circle by Pd atom circle. The effect of subsurface replacing is not regular. The regularity of the replacing effect for the M−O bond is also not found. For the Mulliken charge $q(O)$, it is increased when replacing the two central Pt atoms by Pd atoms and decreased when replacing the surrounding Pt atom circle by Pd atom circle. No observable charge difference can be seen when replacing the subsurface Pt layer by Pd layer. For the Mulliken charge $q(H)$, no observable regularity of replacement effect can also be seen.

In the case of oxygen adsorption, the stronger O adsorption occurs when replacing the two central Pt atoms by Pd atoms, replacing the surrounding Pt atom circle by Pd atom circle, and replacing five subsurface Pd layer by Pt layer. The oxygen−surface length O−S is reduced when replacing two central Pt atoms by Pd atoms and replacing subsurface Pt layer by Pd layer. No observable regularity of surrounding effect can be found. For the Mulliken charge $q(O)$, it is decreased when replacing the two central Pt atoms by Pd atoms. No observable regularity of surrounding and subsurface effect can be found.

In summary, the adsorption energies of OOH and OH are reduced upon replacing the two central Pt atoms by Pd atoms or the subsurface Pt layer by Pd layer and enhanced upon replacing the surrounding Pt atom circle by Pd atom circle. The adsorption energy of O is enhanced upon replacing the two central Pt atoms by Pd atoms or the surrounding Pt atom circle by Pd atom circle and reduced after replacing the subsurface Pt layer by Pd layer. It can be found that Pt-surrounded Pd configuration $Pt_{8,0}Pd_{2,5}$ (D) configuration weakens the OH adsorption the most and thus reduces the poisoning of ORR active site. Although the O adsorption strength on the configuration D is slightly enhanced compared to pure Pt configuration, the adsorption strength is

Table 5. Adsorption Energy (eV), Charge, Fermi Level (eV), and d-Band Center Difference (eV) between Two Different Alloy Configurations ($E_Y - E_X$)

config. X → config. Y	OOH	OH	O	q(M)[a]	Fermi level difference	d-band center difference
			Center Effect			
$Pt_{10,5} \rightarrow Pt_{8,5}Pd_{2,0}$	0.12	0.23	−0.18	0.42	−0.06	0.58
$Pt_{10,0}Pd_{0,5} \rightarrow Pt_{8,0}Pd_{2,5}$	0.30	0.60	−0.09	0.39	−0.04	0.51
$Pt_{2,5}Pd_{8,0} \rightarrow Pt_{0,5}Pd_{10,0}$	−0.01	0.19	−0.01	0.17	0.09	0.42
$Pt_{2,0}Pd_{8,5} \rightarrow Pd_{10,5}$	0.07	0.25	−0.26	0.11	−0.04	0.36
			Surrounding Effect			
$Pt_{10,5} \rightarrow Pt_{2,5}Pd_{8,0}$	−0.34	−0.38	−0.69	−0.48	0.44	0.23
$Pt_{8,5}Pd_{2,0} \rightarrow Pt_{0,5}Pd_{10,0}$	−0.47	−0.42	−0.52	−0.15	0.59	0.07
$Pt_{10,0}Pd_{0,5} \rightarrow Pt_{2,0}Pd_{8,5}$	−0.23	−0.30	−0.41	−0.58	0.53	0.29
$Pt_{8,0}Pd_{2,5} \rightarrow Pd_{10,5}$	−0.46	−0.64	−0.59	−0.86	0.53	0.14
			Subsurface Effect			
$Pt_{10,5} \rightarrow Pt_{10,0}Pd_{0,5}$	0.12	0.14	−0.05	0.27	0.12	0.24
$Pt_{8,5}Pd_{2,0} \rightarrow Pt_{8,0}Pd_{2,5}$	0.30	0.51	0.05	0.24	0.14	0.17
$Pt_{2,5}Pd_{8,0} \rightarrow Pt_{2,0}Pd_{8,5}$	0.23	0.22	0.23	0.18	0.21	0.30
$Pt_{0,5}Pd_{10,0} \rightarrow Pd_{10,5}$	0.31	0.28	−0.02	0.12	0.08	0.24

[a] The Mullikan charge differences of bare center metal atoms between two configurations.

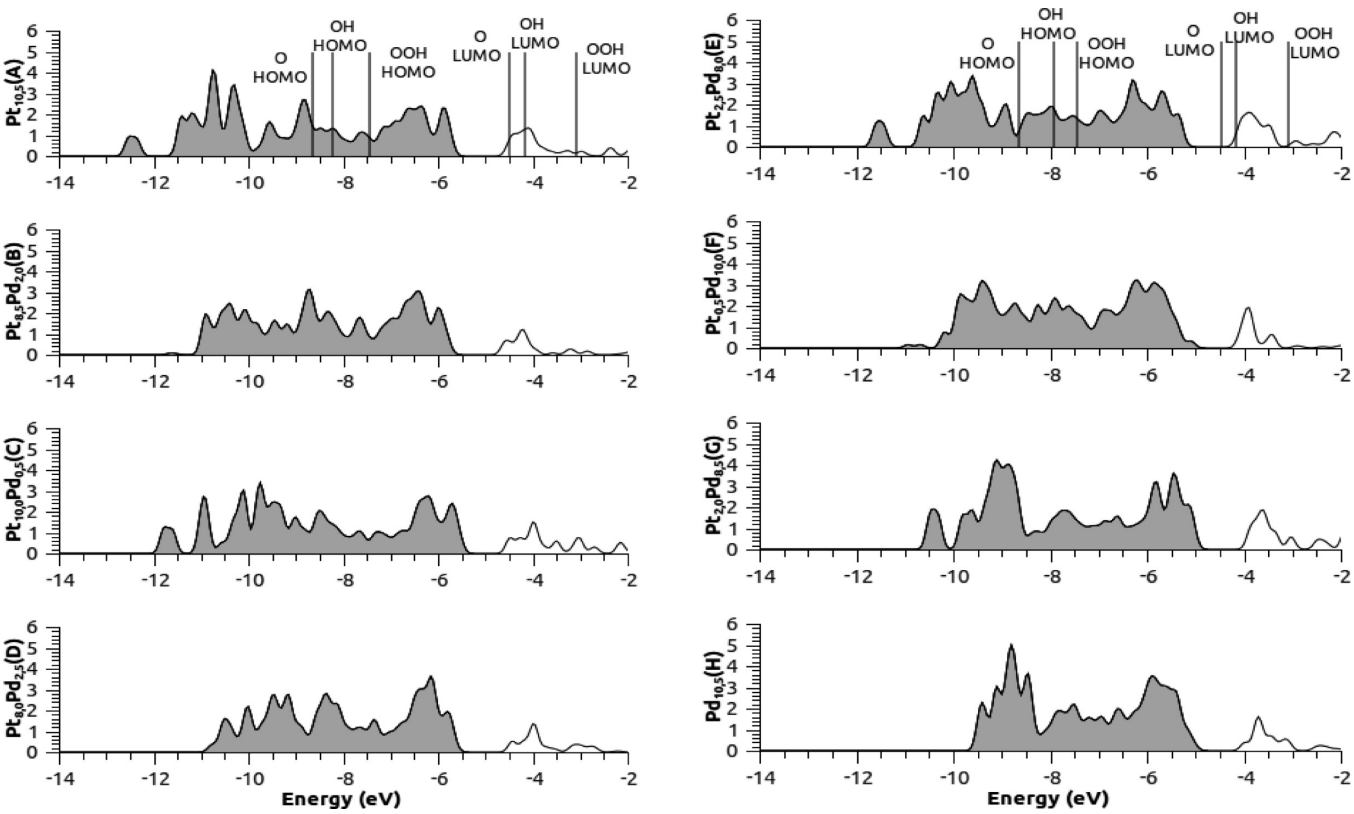

Figure 4. Atom-projected density of states for two central metals of Pt−Pd alloy cluster along with energy levels of HOMO and LUMO of O, OH, and OOH. The black solid region is the occupied density of states, and the hollow region is the unoccupied density of states.

also much weaker than that on Pd-surrounded configurations. Hence, the Pt-surrounded Pd configuration D may be the best choice for ORR.

Center-, surrounding-, and subsurface-replacement effects are sorted and summarized in Table 5. The Fermi level was defined as the middle between the HOMO and LUMO energy level. The Fermi level and charge differences between different configurations are listed in Table 5. It can be found that the shifts of Fermi level for the same kind of configuration substitution are similar. The large difference of Fermi level exists for the surrounding Pt atoms replaced by Pt atoms and corresponds to the adsorption energy enhancing. Because the LUMO energies of O(−4.18 eV),

dx.doi.org/10.1021/jp2000859 |J. Phys. Chem. C 2011, 115, 9105–9116

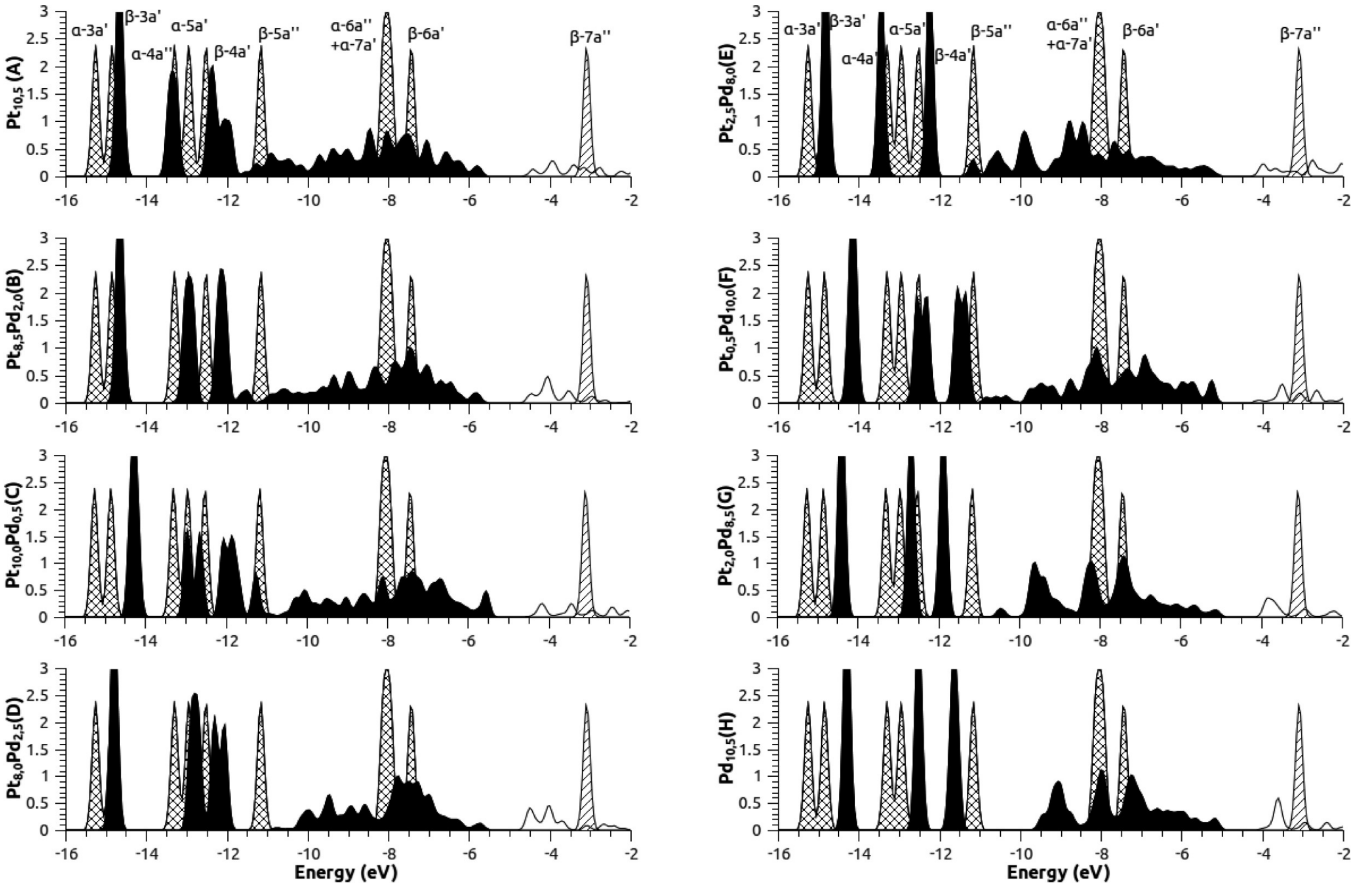

Figure 5. Atom-projected density of states for adsorbed OOH and isolated OOH on Pt−Pd alloy clusters. The black solid, hollow, cross-line, and oblique-line regions are for the occupied adsorbed OOH density of states, unoccupied adsorbed OOH density of states, occupied isolated OOH density of states, and unoccupied isolated OOH density of states, respectively.

OH(−4.48 eV), and OOH(−3.09 eV) are higher than the Fermi levels of Pt−Pd alloy cluster(−4.5 eV∼−5.2 eV), the differences between the LUMO energy and Fermi level are decreasing with the Fermi energy raising, and thus may increase the adsorption energies.

The atom-projected d-band center of alloy cluster for center two metals is also analyzed in the calculation. The definition of d-band center d_c is obtained according to

$$d_c = \frac{\sum_i D_c(E_i)E_i}{\sum_i D_c(E_i)} - E_F \qquad (4)$$

where D_c is the atom-projected density of state for the two central metal atoms. As can be seen in Table 5, the d-band center differences are in the range of 0.36−0.58 when replacing the two central Pt atoms by Pd atoms, in the range of 0.17−0.30 when replacing the eight surrounding Pt atoms by Pd atoms, and in the range of 0.07−0.29 when replacing the five subsurface Pt atoms by Pd atoms. No observables dependency between the adsorption energy and d-band center can be seen.

The charge differences of the two central metal atoms between two configurations are also listed in Table 5. As can be seen in Table 5, replacing the two central Pt atoms by Pd leads to larger Mulliken charges and thus reduces the OOH and OH adsorption. Replacement of subsurface Pt layer by Pd layer also has the same effect. However, replacing the surrounding Pt atom circle by Pd atom circle has the opposite effect, i.e., smaller Mulliken charges and enhanced adsorption.

3.3. The Projected Density of State Analysis of Alloy Local Electronic Structure. Figure 4 shows the atom-projected density of states for the two central atom of eight different alloy clusters. By comparing Figure 4A and Figure 4H, one can notice that between −12 and −10 eV, no density of states can be found for pure Pd cluster compared to those for pure Pt cluster. For pure Pt cluster, the energy states within the range of −12 to −10 eV belong to the mix of Pt 6s and 5d orbitals. Upon replacing the two central Pt atoms by Pd atoms in configurations B, D, F, and G, the contributions of s orbitals in the density of states between −12 and −10 eV are evidently reduced.

In the range of −10 eV to Fermi level, it belongs to the region of pure d-band. These d-band orbitals can donate electrons via interaction with adsorbate LUMO orbitals. It can be found that the d-band is shifted up about 0.5 eV upon replacing surrounding Pt atom circle by Pd atom circle. Upon replacing two central Pt atoms by Pd atoms and replacing subsurface Pt layer by Pd layer, the differences are not remarkable.

In the range of −5 to −3 eV, there are unoccupied metal orbitals. These orbitals mainly come from the vacuum 4s (Pd) or 5s (Pt) orbitals, and little d contributions. Electrons can be back-donated from adsorbate to metal through the interaction between these unoccupied metal orbitals and adsorbate HOMO orbital. It can be found that the unoccupied metal orbitals are also shifted up ca. 0.5 eV upon replacing surrounding Pt atom circle

dx.doi.org/10.1021/jp2000859 |J. Phys. Chem. C 2011, 115, 9105–9116

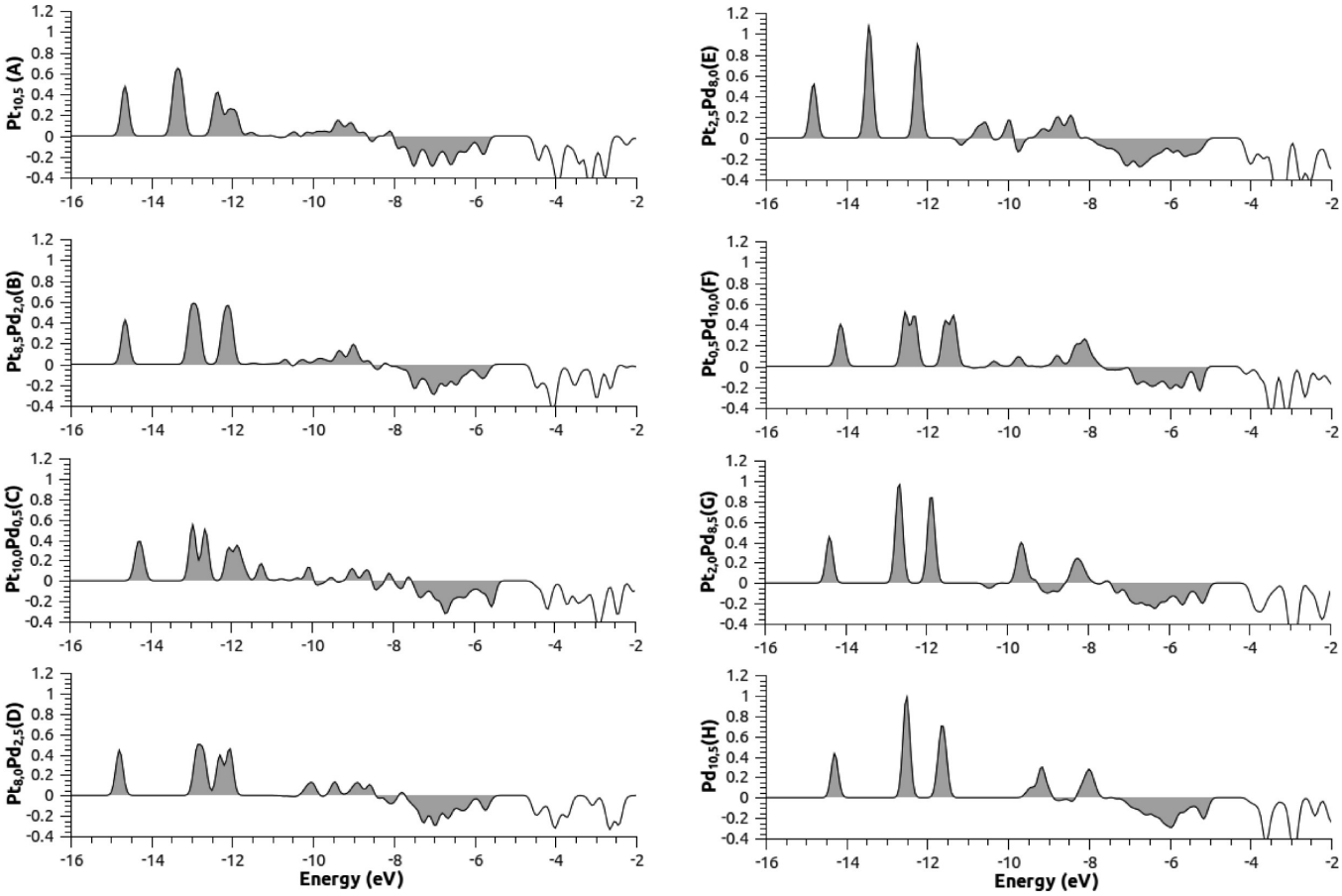

Figure 6. Metal−OOH overlap population density of states for the OOH adsorption on Pt−Pd alloy clusters. The black solid region is the occupied OP density of states, and the hollow region is the unoccupied OP density of states.

Table 6. Total Overlap Population (OP), Bonding Overlap Population, and Antibonding Overlap Population between the Metal Cluster and Adsorbates OOH, OH, and O

	metal−OOH			metal−OH			metal−O		
	total OP	bonding OP	antibonding OP	total OP	bonding OP	antibonding OP	total OP	bonding OP	antibonding OP
$Pt_{10,5}$ (A)	0.231	0.722	0.491	0.290	0.610	0.320	0.514	0.964	0.450
$Pt_{8,5}Pd_{2,0}$ (B)	0.256	0.690	0.434	0.278	0.581	0.303	0.522	1.010	0.488
$Pt_{10,0}Pd_{0,5}$ (C)	0.229	0.730	0.501	0.292	0.613	0.321	0.504	0.951	0.447
$Pt_{8,0}Pd_{2,5}$ (D)	0.226	0.639	0.413	0.260	0.587	0.327	0.520	1.022	0.502
$Pt_{2,5}Pd_{8,0}$ (E)	0.265	0.796	0.531	0.316	0.647	0.331	0.526	0.967	0.441
$Pt_{0,5}Pd_{10,0}$ (F)	0.368	0.750	0.382	0.357	0.612	0.255	0.559	0.971	0.412
$Pt_{2,0}Pd_{8,5}$ (G)	0.270	0.756	0.486	0.342	0.664	0.322	0.564	0.980	0.416
$Pd_{10,5}$ (H)	0.324	0.732	0.408	0.370	0.617	0.247	0.576	0.990	0.414

by Pd atom circle. Upon replacing two central Pt atoms by Pd atoms and replacing subsurface Pt layer by Pd layer, the differences are small and not remarkable.

According to above discussion, it can be found that upon replacing surrounding Pt atom circle by Pd atom circle, the Fermi level is blue-shifted up ca. 0.5 eV and both the occupied d-band and the unoccupied s and d orbitals are also blue-shifted up ca. 0.5 eV. It would lead to a smaller energy difference between d-band and adsorbate LUMO orbital and thus enhance the interaction between occupied metal d band and adsorbate LUMO orbital. However, it also increases the energy difference between the unoccupied metal orbitals and adsorbate HOMO orbital and thus reduces the interaction between adsorbate HOMO and unoccupied metal band. More detail analyses are given in the following section, and the underlying effects of these changes on density of states upon different type of replacement on the adsorption behavior will be discussed.

3.4. The Projected Density of State Analysis of Adsorbates OOH, OH, and O. Figure 5 is the atom-projected density of states for adsorbed OOH and isolated OOH. As can be seen in Figure 5, the interaction between the OOH and pure Pt cluster can be separated into different interaction parts. The first part is that of

dx.doi.org/10.1021/jp2000859 |J. Phys. Chem. C 2011, 115, 9105–9116

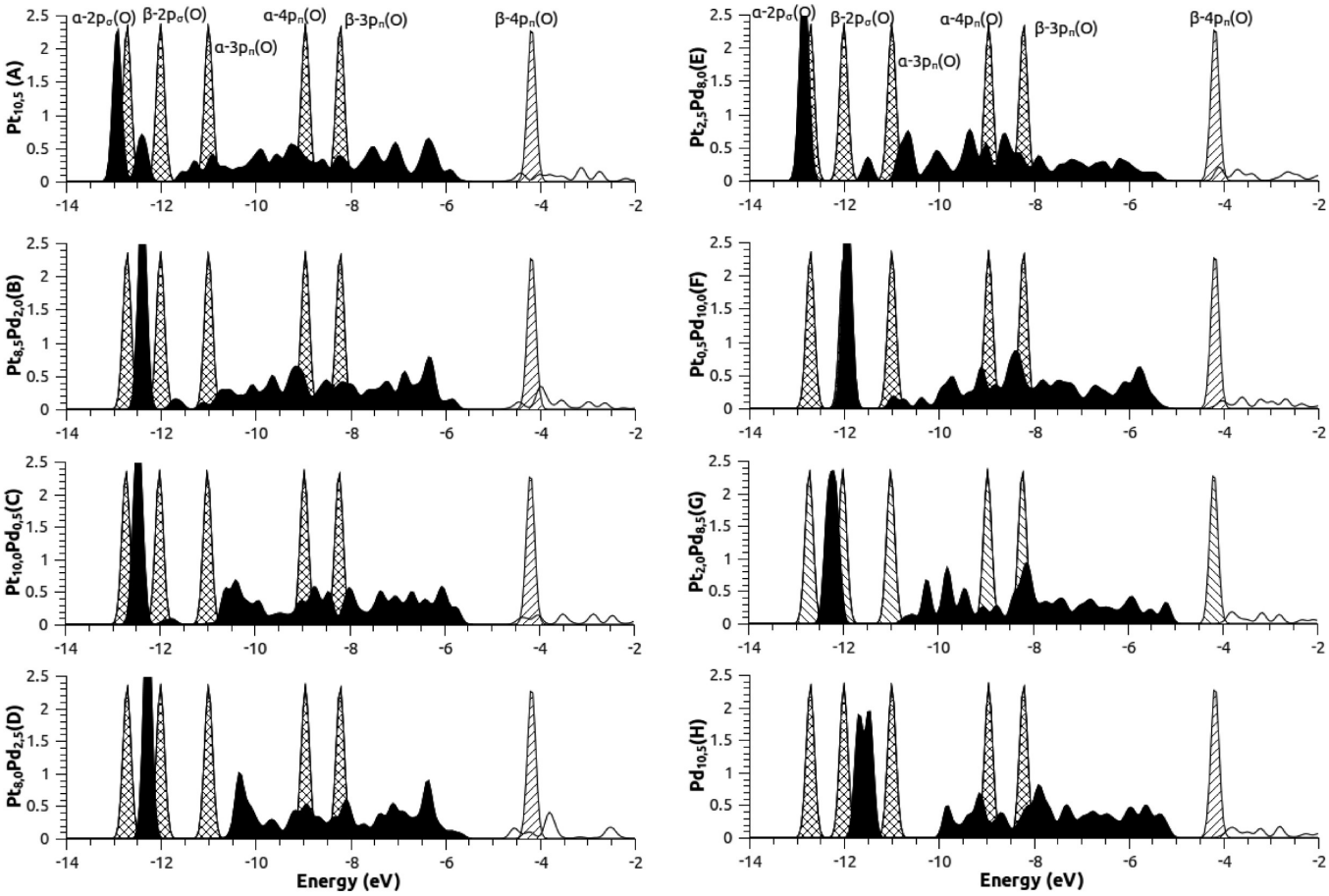

Figure 7. Atom-projected density of states for OH on Pt−Pd alloy clusters. The black solid, hollow, cross-line, and oblique-line region are for the occupied adsorbed OH density of states, unoccupied adsorbed OH density of states, occupied isolated OH density of states, and unoccupied isolated OH density of states, respectively.

the internal OOH orbitals, i.e., the α-3a′, β-3a′, α-4a″, α-5a′, β-4a′, and β-5a″ orbitals, interacting with the occupied metal s and d_z^2 orbitals occurring in the range of −16 to −10 eV. In order to further analyze the OOH−metal interaction, the orbital overlap population (OP) density of states between the OOH and metal is analyzed and shown in Figure 6. The result of OP density of states shows the strong bonding character occur in the range of −16 to −10 eV. Although there are strong bonding characters in this region, it does not directly contribute to the interaction between the OOH and metal because the interaction between two occupied orbitals is repulsive and the corresponding strong antibonding character via the interaction between two occupied orbitals is in the range of −8 eV to Fermi level. The second part is that of the frontier occupied OOH orbitals interacting with the unoccupied metal band and the OOH LUMO orbital interacting with the metal d-band occurring in the range of −10 to −8 eV, which is found to be the major interaction region corresponding to the interaction between OOH and metal. It can be found that the OP density of states in this range is increased upon replacing surrounding Pt atom circle by Pd atom circle and corresponds to the enhancement of OOH adsorption. The third part is that the antibonding region lies in the range of −8 eV to Fermi level. It comes from the antibonding interaction between the internal OOH orbital and occupied metal band.

The total overlap population (see Table. 6) is computed to further characterize the replacement effect on adsorption of interaction. It has been defined as the integration of the overlap population from −16 eV to the Fermi level. Besides, total bonding (positive) OP and total antibonding (negative) OP are also calculated by integration over the positive overlap population and negative overlap population region, respectively. It is found that the metal−OOH bonding OP value for the Pt-surrounded Pd configuration $Pt_{8,0}Pd_{2,5}$ (D) is less than that of other configurations. Although the metal−OOH antibonding OP values are also found to be small, the OOH-projected density of states aggregate in the range of −8 to −6 eV, corresponding to the antibonding region. Thus, the OOH does not favor to adsorb on Pt-surrounded Pd configuration. The strongest interactions occur in the OOH adsorption on the Pd-skin configuration $Pt_{0,5}Pd_{10,0}$ (F) and Pd-surrounded Pt configuration $Pt_{2,5}Pd_{8,0}$ (E). It is found that the metal−OOH bonding OP value for the Pd-skin configuration $Pt_{0,5}Pd_{10,0}$ (F) is larger than that of other configurations. Although the metal−OOH antibonding OP values are large, the OOH-projected density of states aggregate in the range of −12 to −8 eV corresponding to the bonding region. Thus the OOH favors to adsorb on this configuration. For the Pd-surrounded Pt configuration $Pt_{2,5}Pd_{8,0}$ (E), the smallest metal−OOH antibonding OP value and stronger metal−OOH bonding OP value has been obtained, and these values correspond to the strongest OOH adsorption.

Upon replacing the two central Pt atoms by Pd atoms, it can be found that the metal−OOH bonding OP values are decreased,

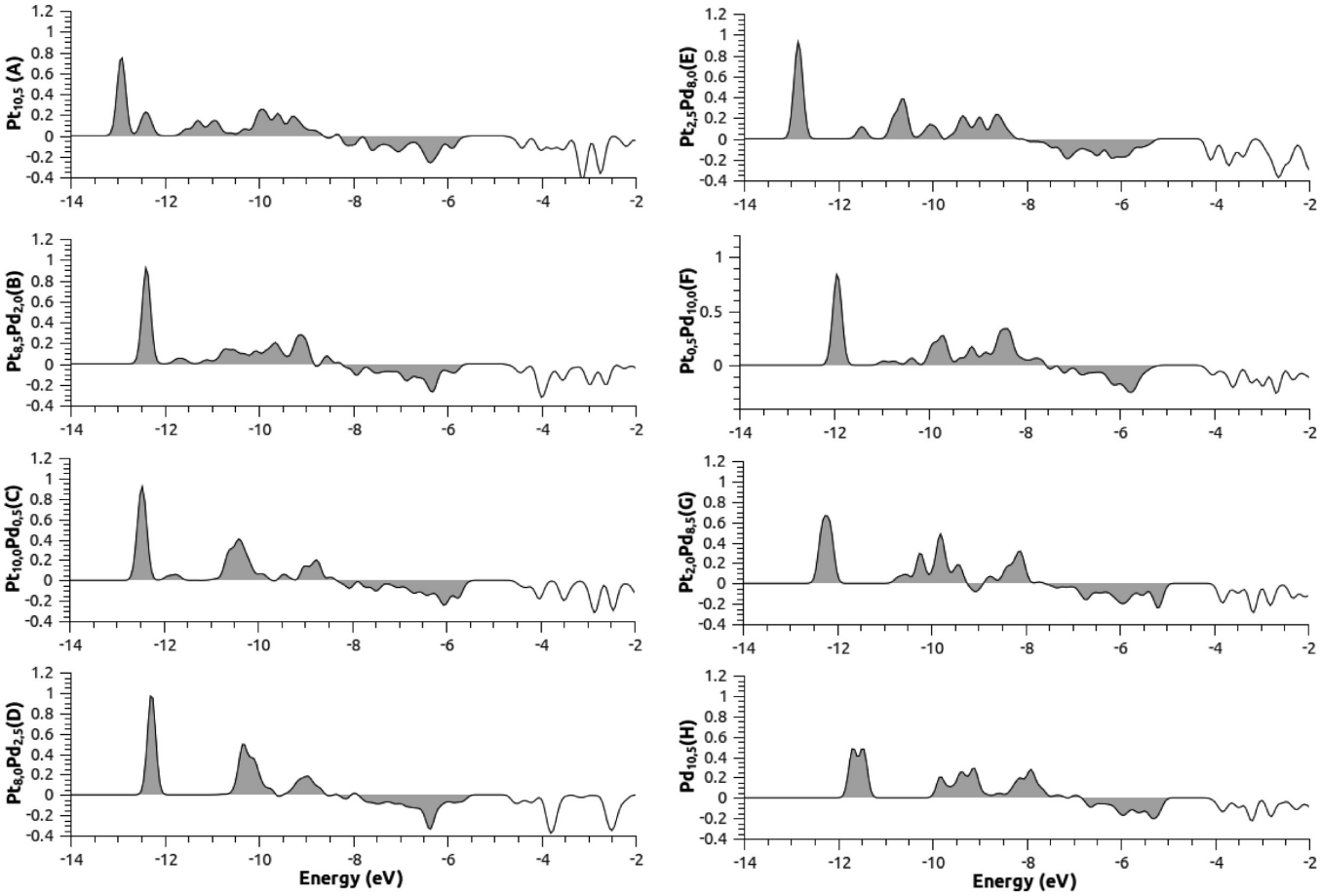

Figure 8. Metal−OH overlap population density of states for the OH adsorption on Pt−Pd alloy clusters. The black solid region is the occupied OP density of states, and the hollow region is the unoccupied OP density of states.

and the metal−OOH antibonding OP values are also decreased. The total metal−OOH OP values are found to be increased after replacing the two central Pt atoms by Pd atoms. However, the influences of bonding OP values are larger than that of metal−OOH antibonding OP values, because the density of states of bonding is larger than those of antibonding. Thus, the difference of OOH adsorption energy is not observable except for the configuration change from C to D owing to the state aggregation in the special case of configuration D. Upon replacing the surrounding Pt atom circle by Pd atom circle, it is found that both the total metal−OOH OP value and metal−OOH bonding OP value are increased. The aggregation of OOH-projected density of states in the bonding region can also be found after replacing the surrounding Pt atom circle by Pd atom circle, thus enhancing the OOH adsorption. Upon replacing the subsurface Pt layer by Pd layer, the metal−OOH bonding OP values are decreased except for the configuration change from A to C corresponding to the small change of the metal−OOH bonding OP value, metal−OOH antibonding OP value, and adsorption energy. Although the enhancement of the metal−OOH bonding OP for the configuration change of F to H is larger than that of B to D and E to G, the metal−OOH antibonding OP is increased after replacing the subsurface Pt layer by Pd layer and thus weakens the OOH adsorption more.

Figure 7 and 8 are the atom-projected density of states for adsorbed OH and isolated OH, and the overlap population density of states between the metal cluster and OH. As can be seen in Figure 7 and 8, the interaction between OH and pure Pt cluster can also be separated into different parts. The first part is that of the internal OH orbitals α-2p_σ and β-2p_σ interacting with the localized metal s and d_z^2 orbitals occurring in the range of −14 to −12 eV. The second part is that of the middle OH orbital α-3p_π and some frontier orbitals α-3p_π and β-3p_π interacting with the occupied metal d-band occurring in the range of −12 to −10 eV. These interactions between two occupied orbitals do not directly contribute to the OH adsorption strength. The third part is that of the frontier OH orbitals α-3p_π and β-3p_π interacting with the unoccupied metal band and the OH LUMO orbital β-4p_π interacting with the occupied metal d-band occurring in the range of −10 to −8 eV. The last part is that the antibonding region lies in the range of −8 eV to Fermi level. It comes from the antibonding interaction between the occupied OH orbital and occupied metal band. Upon replacing Pt atoms by Pd atoms, it can be found the interaction range is shifted, and thus the demarcation between the second part and third part is not very clear in configurations B, E, and F. The total OP analysis can help us further discuss the effects of local configuration.

The total, bonding, and antibonding overlap populations for metal cluster and OH are shown in Table 6. It can be found that that the total OP value for the Pt-surrounded Pd configuration $Pt_{8,0}Pd_{2,5}$ (D) is less than that of other configuration, and the smaller metal−OH bonding OP value and larger metal−OH antibonding OP value can also be seen for the Pt-surrounded Pd

dx.doi.org/10.1021/jp2000859 |J. Phys. Chem. C 2011, 115, 9105–9116

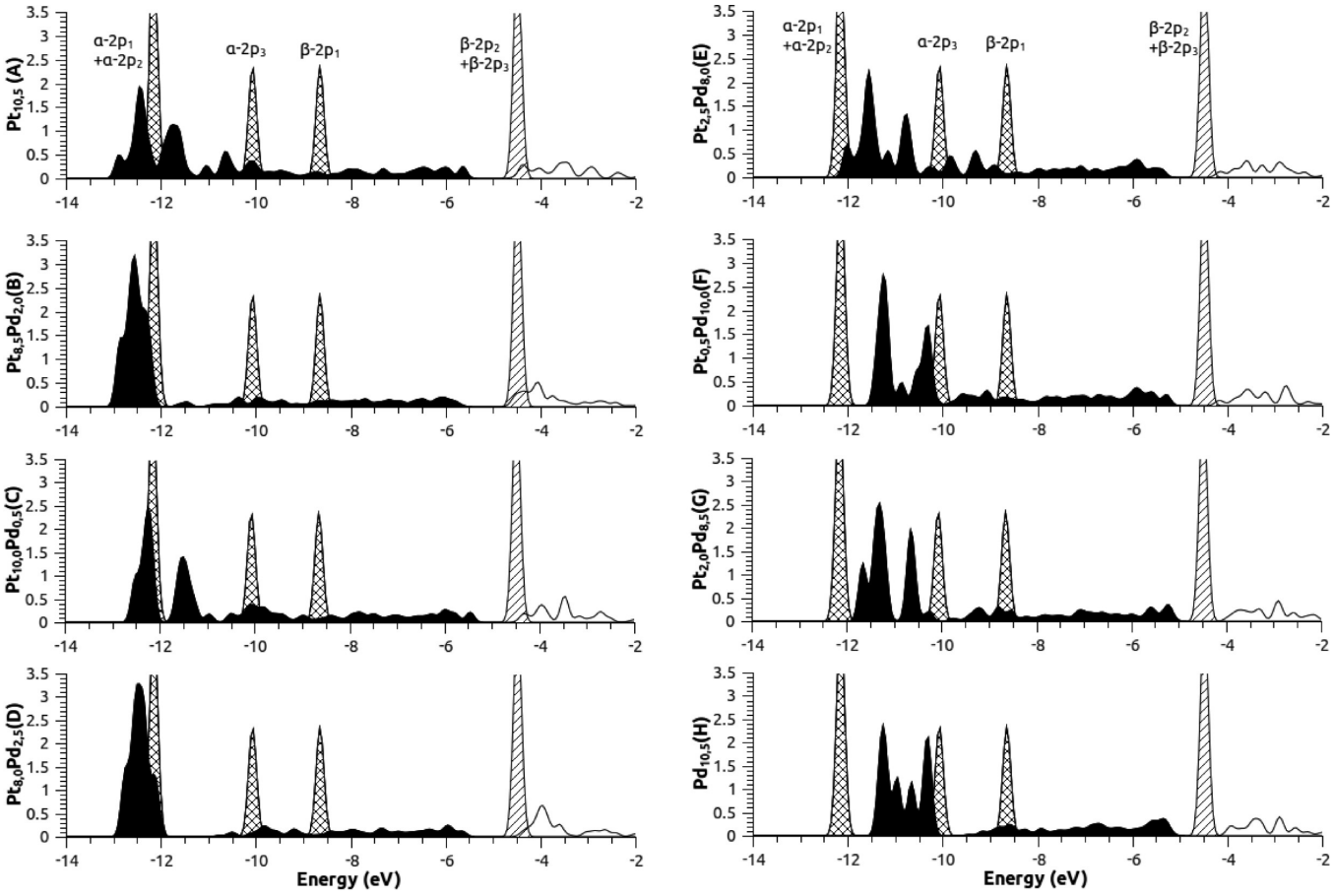

Figure 9. Atom-projected density of states for oxygen on Pt−Pd alloy clusters. The black solid, hollow, cross-line, and oblique-line region are for the occupied adsorbed oxygen density of states, unoccupied adsorbed oxygen density of states, occupied isolated oxygen density of states, and unoccupied isolated oxygen density of states, respectively.

configuration $Pt_{8,0}Pd_{2,5}$ (D). The atom-projected density of states for OH also shows the OH-projected density of states aggregates in the antibonding region. Hence, the interaction between the OH and $Pt_{8,0}Pd_{2,5}$ (D) is weakest. On the contrary, the metal−OH bonding OP of Pd-surrounded Pt configuration $Pt_{2,5}Pd_{8,0}$ (E) is larger than that of other configurations. Although the metal−OH antibonding OP is also large, the OH-projected density of states in the antibonding region is very small. Thus, the OH adsorption favors to adsorb on the Pd-surrounded Pt configuration $Pt_{2,5}Pd_{8,0}$ (E).

Upon replacing the two central Pt atoms by Pd atoms, it can be found that the metal−OH bonding OP values are decreased. The results also show the metal−OH antibond OP values are largely reduced for the Pd surrounding configuration F and G. Although the antibonding OP values are largely decreased for the configuration change from E to F and G to H, it can be observed that the contribution of density of states with antibonding character is small and also reduced after replacing the two central Pt atoms by Pd atoms. Thus the strength of OH adsorption is reduced after replacing. Upon replacing the surrounding Pt atom circle by Pd atom circle, it can be found that the metal−OH bonding OP values are increased and metal−OH antibonding OP values are decreased or unchanged. Thus the strength of OH adsorption is enhanced after replacing the surrounding Pt atom circle by Pd atom circle. Upon replacing the subsurface Pt layer by Pd layer, it can be found that the metal−OH bonding OP values are only slightly changed. However, it is noted that the metal−OH antibonding OP value is increased for the configuration change from B to D, corresponding to the largest reduction in OOH adsorption strength.

Figures 9 and 10 show the atom-projected density of states for adsorbed oxygen and isolated oxygen and the overlap population density of states between the metal cluster and oxygen. It can be found that the bonding picture of O is different from that of OOH and OH. As can be seen in Figures 9 and 10, the O-projected density of states occurring in the range of −14 to −10 eV corresponds to the interaction between the occupied oxygen p orbital and occupied metal d-band, the interaction between the oxygen LUMO p orbital and occupied metal band, and the interaction between the oxygen frontier orbitals and unoccupied metal band. As can be seen in Figure 4, the energy difference between the unoccupied metal d-band and oxygen occupied frontier orbitals is larger than that between the unoccupied metal d-band and occupied OOH/OH frontier orbitals. Thus, the interaction between oxygen LUMO p orbital and occupied metal band is more dominant in the case of oxygen adsorption. In the range of −10 eV to the Fermi level, it can be found that all states in this range possess the antibonding character and the antibonding OP increases with increasing energy.

The total, bonding, and antibonding overlap populations for metal and O interaction are also shown in Table 6. It can be found that the total OP and bonding OP values of metal−O are observably

dx.doi.org/10.1021/jp2000859 |J. Phys. Chem. C 2011, 115, 9105–9116

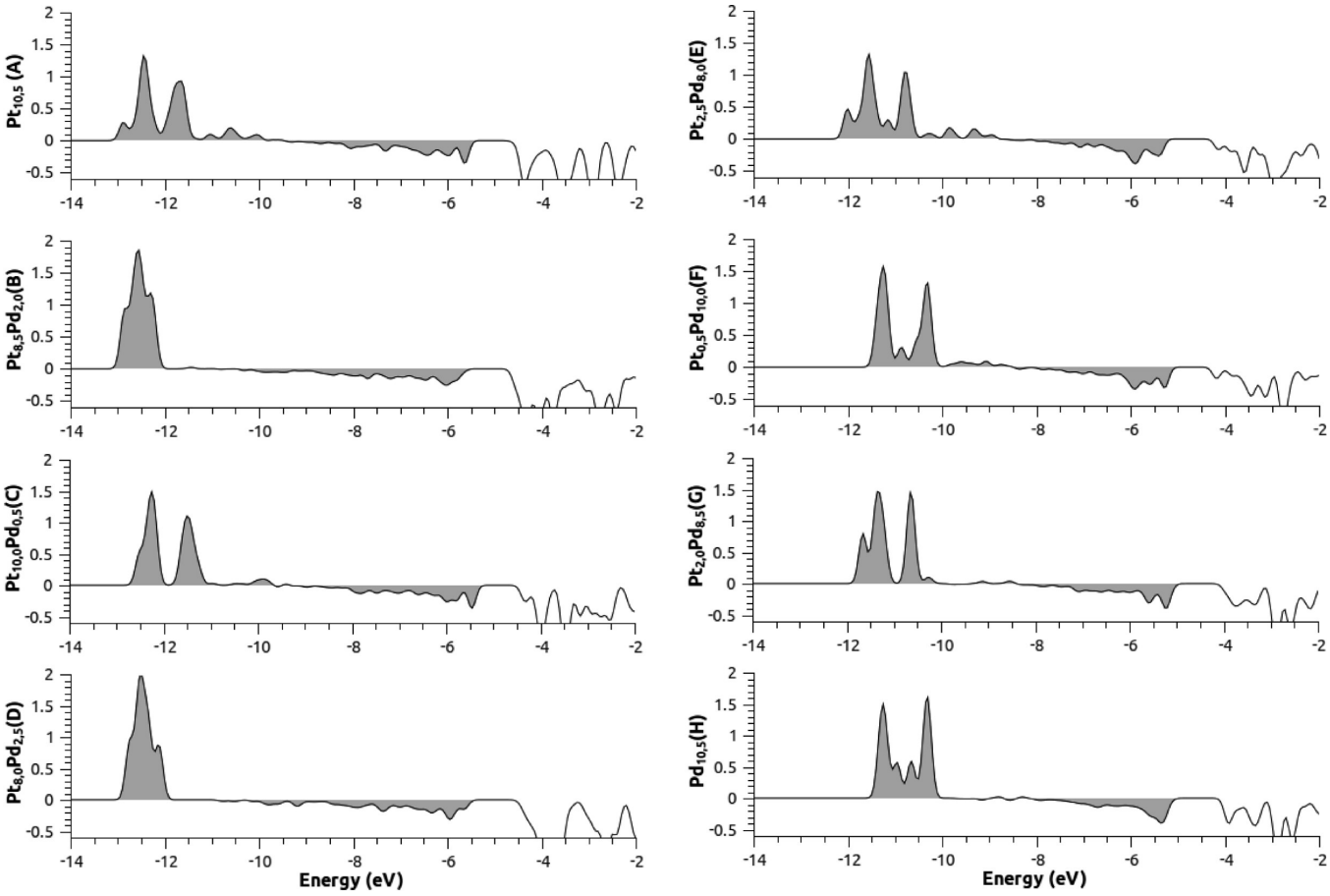

Figure 10. Metal−oxygen overlap population density of states for the oxygen adsorption on Pt−Pd alloy clusters. The black solid region is the occupied OP density of states, and the hollow region is the unoccupied OP density of states.

larger than those of metal−OH and metal−OOH, which imply the stronger interaction between the oxygen and metal cluster. The results of adsorption agree very well with the OP analysis. It can be found the total metal−O OP value for the pure Pd configuration (H) is larger than that for other configurations and thus corresponds to the strongest O adsorption. On the contrary, the total metal−O OP values for the pure Pt configuration (A) and Pt skin configuration $Pt_{10,0}Pd_{0,5}$ (C) are smaller than that for other configurations and thus correspond to the weakest O adsorption.

Upon replacing the two central Pt atoms by Pd atoms, the metal−O total OP value is increased and thus can correspond to the enhancement of oxygen adsorption. However, the metal−O antibonding OP value is also increased upon replacing, and the effect of adsorption enhancement is small. Upon replacing the surrounding Pt atom circle by Pd atom circle, the metal−O total OP value is increased. It can be found that the metal−O antibonding OP value is observably decreased and thus enhances the oxygen adsorption. Upon replacing the Pt layer by Pd layer, it can be found the change of the metal−O total, bonding, and antibonding OP values are small except for the configuration change from E to G. The observation agrees well with the trend of adsorption energy change among different configurations.

4. CONCLUSION

Theoretical investigation for the local electronic alloy effects of OOH, OH, and O adsorption on Pt−Pd alloy clusters has been reported by considering the eight different alloy configurations. The influence of configuration replacing on Pt−Pd alloy cluster has been classified as central, surrounding, and subsurface effect. From our current results, it has been found that the adsorptions of OOH and OH are reduced upon replacing the two central Pt atoms by Pd atoms or the subsurface Pt layer by Pd layer and enhanced upon replacing the surrounding Pt atom circle by Pd atom circle. On the other hand, the adsorptions of O are enhanced upon replacing the two central Pt atoms by Pd atoms or the surrounding Pt atom circle by Pd atom circle and reduced upon replacing the subsurface Pt layer by Pd layer. The different adsorption behavior can be rationalized by examining their bonding picture through analysis of the atom-projected density of states and overlap population density of states. The Pt-surrounded Pd configuration D may be the best choice for ORR since it weakens the OH adsorption the most and thus reduces the poisoning of ORR active site.

■ ASSOCIATED CONTENT

Supporting Information. The total energies of Pt−Pd alloy clusters with respect to different multiplicity and the total energies of OOH, OH, and O adsorption on Pt−Pd alloy clusters. This material is available free of charge via the Internet at http://pubs.acs.org.

AUTHOR INFORMATION

Corresponding Author
*E-mail chesll@ccu.edu.tw; fax +886-5-2721040.

ACKNOWLEDGMENT

We are pleased to acknowledge valuable discussion with Dr. Prabhat K. Sahu. Financial assistance from National Science Council, Taiwan is gratefully acknowledged. We are also grateful to the National Center for High-Performance Computing, Taiwan for computer time and facilities.

REFERENCES

(1) Markovic, N. *Surf. Sci. Rep.* **2002**, *45*, 117.
(2) Stamenkovic, V. R.; Fowler, B.; Mun, B. S.; Wang, G.; Ross, P. N.; Lucas, C. A.; Marković, N. M. *Science* **2007**, *315*, 493.
(3) Nilekar, A. U.; Mavrikakis, M. *Surf. Sci.* **2008**, *602*, L89.
(4) Nørskov, J. K.; Rossmeisl, J.; Logadottir, a.; Lindqvist, L.; Kitchin, J. R.; Bligaard, T.; Jónsson, H. *J. Phys. Chem. B* **2004**, *108*, 17886.
(5) Anderson, A. B.; Roques, J.; Mukerjee, S.; Murthi, V. S.; Markovic, N. M.; Stamenkovic, V. *J. Phys. Chem. B* **2005**, *109*, 1198.
(6) Drillet, J.; Ee, a.; Friedemann, J.; Kotz, R.; Schnyder, B.; Schmidt, V. *Electrochim. Acta* **2002**, *47*, 1983.
(7) Jaouen, F. d. r. *J. Phys. Chem. C* **2009**, *113*, 15433.
(8) Jeon, T.-Y.; Yoo, S. J.; Cho, Y.-H.; Lee, K.-S.; Kang, S. H.; Sung, Y.-E. *J. Phys. Chem. C* **2009**, *113*, 19732.
(9) Marković, N. M.; Schmidt, T. J.; Stamenković, V.; Ross, P. N. *Fuel Cells* **2001**, *1*, 105.
(10) Toda, T. *J. Electrochem. Soc.* **1999**, *146*, 3750.
(11) Toda, T. *J. Electrochem. Soc.* **1998**, *145*, 4185.
(12) Zhang, J.; Mo, Y.; Vukmirovic, M. B.; Klie, R.; Sasaki, K.; Adzic, R. R. *J. Phys. Chem. B* **2004**, *108*, 10955.
(13) Zhang, J.; Vukmirovic, M. B.; Sasaki, K.; Nilekar, A. U.; Mavrikakis, M.; Adzic, R. R. *J. Am. Chem. Soc.* **2005**, *127*, 12480.
(14) Stern, E. *Phys. Rev. B* **1972**, *5*, 366.
(15) Stamenkovic, V. R.; Mun, B. S.; Arenz, M.; Mayrhofer, K. J. J.; Lucas, C. a.; Wang, G.; Ross, P. N.; Markovic, N. M. *Nat. Mater.* **2007**, *6*, 241.
(16) Roques, J. r. m.; Anderson, A. B. *J. Electrochem. Soc.* **2004**, *151*, E85.
(17) Xu, Y.; Ruban, A. V.; Mavrikakis, M. *J. Am. Chem. Soc.* **2004**, *126*, 4717.
(18) Gu, Z.; Balbuena, P. B. *J. Phys. Chem. C* **2008**, *112*, 5057.
(19) Calvo, S. R.; Balbuena, P. B. *Surf. Sci.* **2007**, *601*, 4786.
(20) Kitchin, J. R.; Nørskov, J. K.; Barteau, M. a.; Chen, J. G. *J. Chem. Phys.* **2004**, *120*, 10240.
(21) Sepa, D. B.; Vojnovic, M. V.; Damjanovic, A. *Electrochim. Acta* **1981**, *26*, 781.
(22) Sepa, D. B.; Vojnovic, M. V.; Vracar, L. M.; Damjanovic, A. *Electrochim. Acta* **1987**, *32*, 129.
(23) Becke, A. D. *J. Chem. Phys.* **1993**, *98*, 5648.
(24) Dill, J. D. *J. Chem. Phys.* **1975**, *62*, 2921.
(25) Hay, P. J.; Wadt, W. R. *J. Chem. Phys.* **1985**, *82*, 299.
(26) Antolini, E. *Energy Environ. Sci.* **2009**, *2*, 915.
(27) Frisch, M. J.; Trucks, G. W.; Schlegel, H. B.; Scuseria, G. E.; Robb, M. A.; Cheeseman, J. R.; Scalmani, G.; Barone, V.; Mennucci, B.; Petersson, G. A.; Nakatsuji, H.; Caricato, M.; Li, X.; Hratchian, H. P.; Izmaylov, A. F.; Bloino, J.; Zheng, G.; Sonnenberg, J. L.; Hada, M.; Ehara, M.; Toyota, K.; Fukuda, R.; Hasegawa, J.; Ishida, M.; Nakajima, T.; Honda, Y.; Kitao, O.; Nakai, H.; Vreven, T.; Montgomery, J. A., Jr.; Peralta, J. E.; Ogliaro, F.; Bearpark, M.; Heyd, J. J.; Brothers, E.; Kudin, K. N.; Staroverov, V. N.; Kobayashi, R.; Normand, J.; Raghavachari, K.; Rendell, A.; Burant, J. C.; Iyengar, S. S.; Tomasi, J.; Cossi, M.; Rega, N.; Millam, N. J.; Klene, M.; Knox, J. E.; Cross, J. B.; Bakken, V.; Adamo, C.; Jaramillo, J.; Gomperts, R.; Stratmann, R. E.; Yazyev, O.; Austin, A. J.; Cammi, R.; Pomelli, C.; Ochterski, J. W.; Martin, R. L.; Morokuma, K.; Zakrzewski, V. G.; Voth, G. A.; Salvador, P.; Dannenberg, J. J.; Dapprich, S.; Daniels, A. D.; Farkas, Ö.; Foresman, J. B.; Ortiz, J. V.; Cioslowski, J.; Fox, D. J. *Gaussian 03*, revision E01; Gaussian, Inc.: Wallingford, CT, 2003.
(28) Gorelsky, S. *J. Organomet. Chem.* **2001**, *635*, 187.
(29) Gorelsky, S. I. AOMix: Program for Molecular Orbital Analysis, http://www.sg-chem.net/, University of Ottawa, version 6.4, 2010.